Impact generating mechanisms in damaged rolling element bearings

Sarabjeet Singh (1), Uwe Köpke (2), Carl Howard (1), Dick Petersen (1) and David Rennison (2)

(1) School of Mechanical Engineering, The University of Adelaide, South Australia, Australia
(2) Trackside Intelligence Pty Ltd, 17-19 King William St, Kent Town, SA, Australia

ABSTRACT

Standard condition monitoring techniques for assessing the health of rolling element bearings are widely used in numerous engineering industries. It is well known that the appearance of impulses in measured acceleration signals indicates the presence of a defect within a bearing. Although a large amount of technical content related to the signal processing of measured time-domain signals has been published in the literature and new data analysis methods are continued to be developed and enhanced, the mechanism by which the defect-related impulses are generated has received much less attention and has not been investigated in detail. This paper provides an explanation of the mechanisms by which defect-related impacts are produced in damaged rolling element bearings on the basis of findings from numerical modelling conducted using an explicit dynamics finite element software package, LS-DYNA. In-depth analysis of the numerically obtained impact-contact forces between the rolling elements and raceways of a bearing, which are not measured in practice, are presented in this paper.

INTRODUCTION

Rolling element bearings are widely used in machinery and found in a variety of industries that include aerospace (engine and gearbox bearings), construction and mining, paper mills, railways and renewable energy. The damage and failure of rolling element bearings contribute to machinery breakdown, consequently costing significant economic losses and human lives in certain situations, such as engine failure in aircraft and train derailment due to seizure of a bearing. Standard condition monitoring techniques are often applied to monitor the health of bearings. One of the basic techniques is to measure the acceleration of a bearing at a suitable location (most commonly its outer shell or a pedestal into which a bearing is mounted), and conduct a combination of time-domain, frequency-domain and time-frequency domain analyses. The presence of impulses in measured acceleration time-histories generally indicates the presence of a defect within a bearing.

Numerous publications discuss condition monitoring techniques applicable to defective rolling element bearings. However, the physical mechanism that generates the defect-related impacts in damaged rolling element bearings has attracted much less attention.

For engineers and technicians, who are involved in the condition monitoring of rolling element bearings, the phenomenon by which the defect-related impacts are generated is not important as the detection of such impacts is sufficient for them to assess the health of the bearings. Many researchers have developed analytical models to simulate the vibration response of defective rolling element bearings (McFadden *et al*, 1984, McFadden *et al*, 1985, Su *et al*, 1992, Tandon *et al*, 1997, Sawalhi *et al*, 2008a and 2008b, Patil *et al*, 2010, Rafsanjani *et al*, 2009, Tadina *et al*, 2011). The main emphasis of the existing models is to explain the characteristics of experimentally obtained vibration signals. These mainly include predicting the defect-related fundamental and harmonics.

This paper provides a detailed explanation of the fundamental mechanism of defect-related impacts generation in damaged rolling element bearings. Numerical modelling of a rolling element bearing with a rectangular defect on its outer raceway was conducted using an explicit dynamics finite element software package, LS-DYNA (Hallquist, 2006). The finite element model presented in this paper includes all the components of a bearing, such as the inner and outer rings, rolling elements and cage. An in-depth analysis of the numerically modelled impact-contact forces that are generated as the rolling elements traverse through a raceway defect is presented in this paper.

NUMERICAL MODELLING

The numerical modelling was conducted using the software package, LS-DYNA. It is a multiphysics simulation software package capable of simulating complex dynamics problems, and is used by numerous industries, such as automotive, aerospace, construction, military, manufacturing, and bioengineering industries. LS-DYNA uses an explicit time integration scheme for simulating highly nonlinear transient dynamic events of very short duration. This type of finite element code is different from the implicit dynamics software such as ANSYS and NASTRAN.

Description of the finite element model

A two-dimensional (2-D) finite element model of a rolling element bearing was built using LS-DYNA. The model comprises the following components: an outer ring (more commonly referred to as *cup*), an inner ring (more commonly referred to as *cone*), a cage retaining a total of twenty-four (24) rolling elements, and an adaptor that interface the load to the outer ring. Both rings were 10 mm thick, and the outer radii of outer and inner rings were 110 mm and 82 mm, respectively. The thickness of the cage was 5 mm and its outer radius was 98 mm. There was a nominal radial clearance of 0.02 mm between the rolling elements and the inner (running) surface of the cup, more commonly referred to as *cup*

raceway. The clearance between the rolling elements and their corresponding cage slots was 0.35 mm.

The bearing was modelled with a geometrical rectangular defect on the cup raceway that was located centrally at the top. The dimensions of the defect were 10 mm (circumferential length/width) x 0.1 mm (height/depth). Such a defect is often referred to as a '*line spall*'.

Two-dimensional (2-D) solid elements were used to model the bearing as a solid structure. A 2-D element is defined by four nodes having two degrees of freedom at each node: translations in the nodal x- and y-directions. The elements were modelled as plane strain elements. The isotropic elastic material model was chosen for the analysis, and the material steel was used to model the components with values of density, ρ = 7850 kg/m^3, modulus of elasticity, E = 200 GPa, and Poisson's ratio, ν = 0.3.

All the components within the model were meshed using quadrilateral elements, except the rolling elements which due to their geometry, could not be meshed with the quadrilateral elements. They were, therefore, meshed with a mixture of quadrilateral and triangular elements. As the rolling elements need to establish a continuous rolling contact with the outer and inner raceways, in order to transmit the load between the raceways, the element mesh size was optimally chosen to be 0.5 mm on the basis of numerous simulations undertaken during the course of this research. It is interesting to note that for a transient dynamic finite element structural analysis, it is recommended to use at least 20 elements-per-wavelength (Hallquist, 2006) in order to accurately predict the behaviour of a structure. However, the chosen element mesh size of 0.5 mm corresponds to 97 elements-per-wavelength, which is nearly 5x the recommended elements-per-wavelength criterion.

Figure 1 shows the 2-D finite element mesh of the bearing annotated with the names of the components. The geometrical rectangular defect located centrally at the top of the cup raceway, which cannot be seen in Figure 1, is shown in Figure 2 for clarity.

The following boundary conditions and loads were applied to the finite element model:

- A radial load of 50 kN on the top of the adaptor in the negative (-) y direction was applied so as to radially load the bearing.
- The inner ring (cone) was constantly rotated with a uniform angular velocity of 500 revolutions per minute (rpm) in a clockwise direction.
- In a typical bearing operation, generally, one ring is fixed while the other rotates. In this model, the outer ring was fixed, however no direct constraints could be applied to the outer ring as this would result in constraining its translations and consequently vibrations. In order to overcome this problem, a frictional contact with a high coefficient of friction, 0.1, between the outer ring and adaptor was implemented. The adaptor was translationally constrained in the global x-direction, and as a result of the frictional contact, the outer ring was prevented from being rotated during the simulation.
- A frictional contact between all other components within the model was defined with a very low coefficient of friction as 0.005. This is comparable with that of the frictional coefficient recommended for rolling element bearings.
- A global damping of 2% was applied to the finite element model.
- The standard Earth's gravity was also applied to the finite element model.

The termination time of the numerical simulation was set to 30 milli-seconds. The results, in the form of binary text files, were written at the interval of 0.01 milli-seconds, which corresponds to the sampling rate of 100 kHz. All the LS-DYNA results were post-processed using MATLAB.

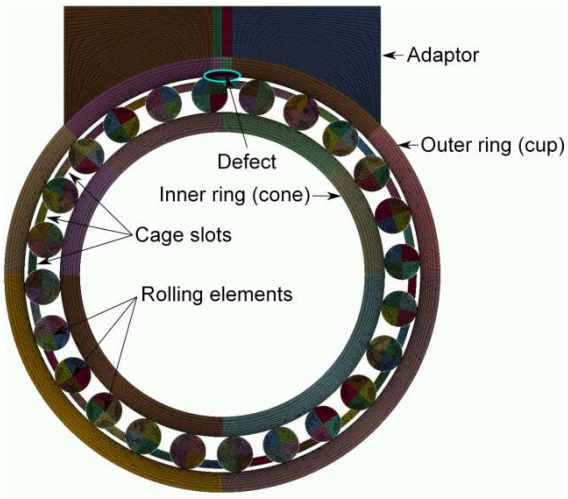

Figure 1: An image of the meshed 2-dimensional finite element model created using LS-DYNA showing the names of all the components within the model. The rectangular defect at the top is shown in Figure 2.

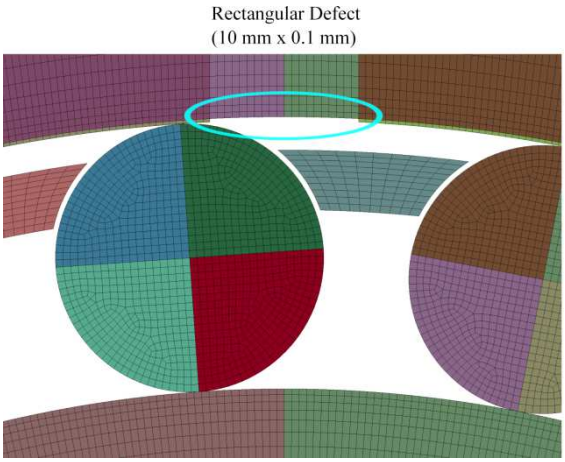

Figure 2: A zoomed image of Figure 1 showing the meshed 2-dimensional finite element model, and the 1 element deep rectangular defect on the running surface of the outer ring highlighted using the ellipse.

Results and observations

A common technique used in vibration condition monitoring of rolling element bearings is the measurement of acceleration levels. Similarly in these simulations, the nodal acceleration results obtained from the numerical modelling using LS-DYNA are presented.

Figure 3 shows the (unfiltered) time-history plot of the numerically (LS-DYNA) obtained acceleration results for a

node located on the outer surface of the cup. The consecutive defect-related impacts, evident in the plot, are separated by approximately 0.011 seconds. The aforementioned time separation corresponds to the outer (cup) raceway defect frequency, commonly referred to as ball pass outer raceway frequency (BPFO), f_{bpo}, of 90.91 Hz. The theoretical estimate of f_{bpo} is given by

$$f_{bpo} = \frac{Z \times f_s}{2}\left(1 - \frac{D}{d_m}\cos(\alpha)\right) \quad (1)$$

where, Z is the number of rolling elements, f_s is the run speed (i.e. the rotational speed of inner ring), D is the rolling element diameter, d_m is the pitch diameter of bearing, and α is the contact angle. For the bearing modelled here, the theoretical estimate of BPFO is 90.19 Hz, which is 0.8% different from the results of the LS-DYNA simulation. The slight difference between the numerical and analytical estimations is due to the reason that the analytical formula, Equation (1), does not consider the slippage of the rolling elements (Ho et al, 2000, Randall et al, 2001). As the numerical modelling of the bearing undertaken here simulated its real-time dynamics, the slippage of the rolling elements was automatically accounted during the solution.

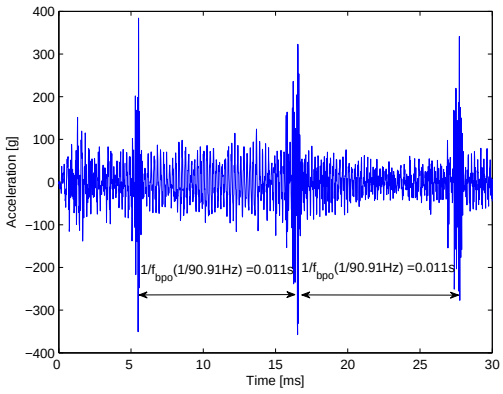

Figure 3: Numerically (LS-DYNA) modelled acceleration results for a node located on the outer surface of the cup of the 2-D finite element bearing model for the bearing run speed of 500 rpm.

A close agreement between the numerical and theoretical estimates of the cup defect frequency shows that the LS-DYNA model has simulated the basic bearing kinematics satisfactorily. However, the acceleration signal has a substantial amount of noise that is explained in the following section.

Contact noise: an artefact of numerical modelling

It can be observed from Figure 3 that while the peak impulsive acceleration levels for the three visible defect-related impacts range from 100 g to 400 g, the non-impulsive acceleration levels between the impacts are of the order of 100 g. It is understood that results from LS-DYNA simulations can contain a significant amount of numerical noise (Hallquist, 2006).

In the model developed here, the two contact interfaces: 1) rolling elements-cup running surface, and 2) rolling elements-cone running surface, generate numerical noise through the solution method of determining the dynamic equilibrium forces, and have contributed significantly to the introduction of noise in the LS-DYNA modelling results. This numerical noise is in addition to the elemental vibration noise which is an inherent feature of LS-DYNA solutions (Hallquist, 2006).

The two noise frequency components present in the numerical acceleration results, shown in Figure 3, are approximately 4761.91 Hz and 4545.45 Hz. These frequency components were found to be the function of the element size used to mesh the geometrical model, and the velocity of the rolling elements during the simulation. The noise frequency components can be estimated using one of the basic equations of motion given by

$$f_{noise} = \frac{1}{t} = \frac{v}{d} = \frac{\omega r}{d} \quad (2)$$

where, d is the distance between two nodes in the finite element model (mesh element size, 0.5 mm), ω is the angular velocity with which the rolling elements roll during the simulation, and r can either be the radius of the cup running surface (100 mm) or cone running surface (82 mm) which contact the rolling elements.

Because the rolling elements were discretised into a number of finite elements, the edges of the rolling elements were transformed from circular to multi-point polygons. As they roll during the simulation, the *polygonised* rolling elements create a little impact upon their contact with the cup and cone raceways. Solving Equation (2) for the values of r as 100 mm and 82 mm, the noise frequencies equal 4712.38 Hz and 3864.15 Hz, respectively.

The comparison of the analytically calculated former noise frequency, 4712.38 Hz, with 4761.91 Hz, one of the dominant noise frequency components present in the numerically modelled acceleration results, indicates that the presence of the numerical noise at 4761.91 Hz is highly likely due to the interaction of the rolling elements with the cup running surface. The error between the analytically calculated noise frequency, 4761.91 Hz, and noise frequency component observed in the numerically modelled acceleration results, 4712.38 Hz, is 1.04%.

Beating phenomenon

The presence of the latter noise frequency component found in the numerically modelled acceleration results, 4545.45 Hz, is due to the `*beating*' effect. As the rolling elements contact both cup and cone raceways during their movement, the *polygonised* edges of the rolling elements create small impacts with both raceways as they roll during the simulation. The interaction of the rolling elements with the raceways would result in the generation of two sinusoidal waves with a slight difference between their carrier frequencies. The amplitude of the sinusoidal waves would also slightly differ from each other. In order to demonstrating the beating effect, the sum of two interfering sinusoidal waves is

$$P(t) = A_1 \cos(2\pi f_1 t) + A_2 \cos(2\pi f_2 t) \quad (3)$$

where, A_1=A_2=1 are the wave amplitudes , t is the time vector, and f_1 and f_2 are the analytically estimated noise frequencies (f_1= 4712.38 Hz and f_2=3864.15 Hz).

Figure 4 shows a resultant sinusoidal wave in the top plot and the same wave along with its envelope, zoomed from 0.009 s to 0.015 s for clarity, in the bottom plot. The time-separation of the two consecutive peaks, whose data cursors are shown in the bottom plot, corresponds to 4545.45 Hz. This frequency exactly matches the other noise frequency component observed in the numerically (LS-DYNA) modelled accelera-

tion results. The beating effect can also be clearly seen in Figure 3 from 0.005 s to 0.015 s.

Although the time-history acceleration plot, shown in Figure 3, clearly shows the defect-related impulsive signals whose frequency also match well with the nominal defect frequency, by viewing the acceleration data, further explanations are required to describe the physical mechanisms by which these impacts are generated and is presented in the following section.

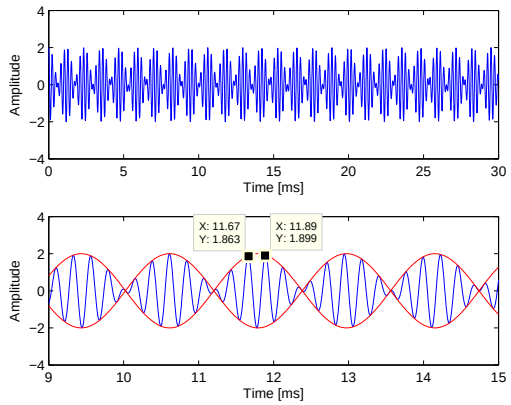

Figure 4: Demonstration of a beating effect due to the interference of two sinusoidal waves at the two noise frequencies observed in the numerically (LS-DYNA) modelled acceleration results.

IMPACT-CONTACT ANALYSIS

The term '*impact-contact analysis*' used throughout this paper refers to analysing the contact forces between two contact interfaces; 1) rolling elements-cup raceway, and 2) rolling elements-cone raceway.

Figure 5 shows the numerically (LS-DYNA) modelled contact force plots between the three rolling elements, which traversed through the rectangular defect, and the cup running surface, in a chronological order from top to bottom. The analytically modelled static contact forces on the corresponding rolling elements for a non-defective bearing has also been plotted (using broken lines) along with the numerical modelling results for comparison purposes. The static solution was adapted from a text-book (Harris, 2001).

A good agreement of the numerically modelled contact forces with those of the analytically estimated contact forces on the rolling elements indicates the validation of the numerical modelling. However, like the numerically modelled acceleration results, shown in Figure 3, the numerical contact force results were also contain the numerical noise. The noise frequency components observed in the contact force plots are similar to those observed in the acceleration results. Also, the presence of the beating phenomenon can be observed in the contact force plots.

Three events are highlighted on all the subplots shown in Figure 5. For the purpose of relating these events with the movement of the rolling elements, refer to Figure 6. It shows a schematic of a 2-D bearing model comprising a cup, cone, a few rolling elements and a rectangular defect. The rolling elements marked as '1', '2' and '3' are the ones that traversed through the defect in the clockwise direction during the numerical simulation presented in this paper. The '*starting*' and '*ending*' position of the defect are also shown in the schematic. Throughout the discussion to follow, the '*top surface of the defect*' is referred to as the '*surface of the damaged cup raceway*' as shown in the schematic.

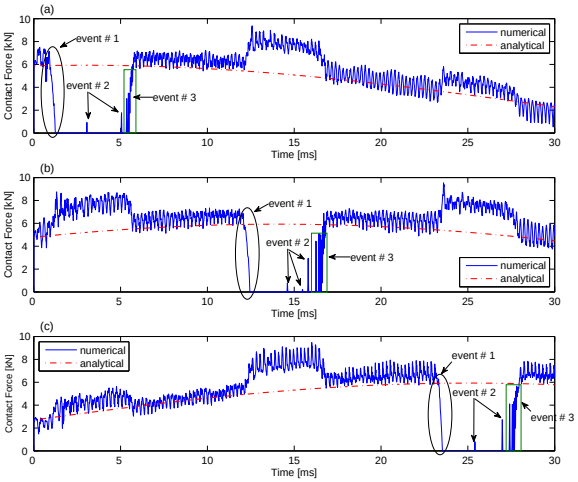

Figure 5: Numerically (LS-DYNA) modelled results for the contact forces between the cup raceway and the three rolling elements that traversed through the defect; (a) cup raceway-rolling element 1, (b) cup raceway-rolling element 2, and (c) cup raceway-rolling element 3.

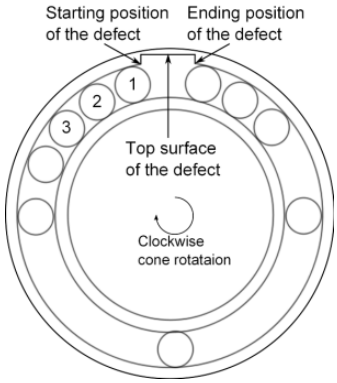

Figure 6: A schematic of a 2-dimensional bearing model showing a cup, a cone, a few rolling elements and a rectangular defect (not to scale).

Event #1: Entry of the rolling elements into the defect – the *de-stressing* phase

The application of a radial load on a bearing results in the loading of a certain number of its rolling elements. As a result, the rolling elements, which are under the influence of load zone, are stressed between the cup and cone raceways. The maximum stress on the rolling elements at their two respective points of contact with cup and cone raceways can be analytically estimated using the classical Hertz's theory (Hertz, 1882).

The results of the numerically modelled contact forces between the rolling elements and cup raceway show that as a stressed rolling element started entering the defect, located on the cup raceway, it gradually started losing contact with the cup raceway. Consequently, the contact force between the rolling element and the cup raceway started decreasing gradually to zero. The reduction of the contact force from approximately 6 kN (for the first rolling element) to 0 kN implies that the rolling element has no mechanical stress in contrast to its location between the raceways.

The gradual drop in the contact force between all the three rolling elements, which traverse through the defect, and the cup raceway is highlighted using solid elliptical markers in all the subplots shown in Figure 5. Event #1, which corresponds to the entry of the rolling elements into the defect, can be referred to as '*de-stressing of the rolling elements*'. The consecutive de-stressing events are separated by 0.011 seconds, which corresponds to the BPFO of 90.91 Hz. It also matches the analytically estimated BPFO with the percentage error of 0.8% between the numerical and analytical solutions.

The numerically modelled contact force results show that the de-stressing of the rolling elements appears to be a (near) step response with no indication of an impact and does not excite a broad range of frequencies which generally causes the ringing of a bearing.

Event #2: Traverse of the rolling elements through the defect

The zero values of the contact force between the rolling elements and the damaged part of the cup raceway indicates that the rolling elements had no contact with the damaged raceway as they traverse through the defect. The numerically (LS-DYNA) modelled contact force results in Figure 5 show that during the traverse of the rolling elements through the defect, the contact force remains zero for most of the time except for a few instances. These instances, which are indicated as *event # 2* on the subplots in Figure 5, correspond to the impact of the rolling elements with the '*top surface of the defect/ damaged part of the cup raceway*'.

During the operation of a bearing, the rolling elements possess centrifugal forces. While the centrifugal forces tend to project the rolling elements outward from the centre of the bearing, their outward trajectory is restricted between the cup and cone raceways when the rolling elements are stressed between the raceways. However, when the rolling elements are de-stressed due to the loss of contact with the cup raceway while they traverse through the defect, they tend to freely follow their outward trajectory. And, at some instance, they impact the top surface of the defect. Such impacts are evident in all the three subplots in Figure 5 and are indicated as event #2.

It can be seen from the subplots in Figure 5 that the first and third rolling elements impact the top surface of the defect twice, while the second rolling element impacts the defect surface three times. It is also interesting to note that not only the amplitudes of these impacts differ from each other but also the timings of the impacts. The reason for the varying period is due to the interaction of the rolling element with the adjacent cage slots. The irregular period of the impact timings implies that at some instances the rolling elements are driven by the cage (slots), and at other instances, the rolling elements drive the cage.

Event #3: Exit of the rolling elements from the defect – the *re-stressing* phase

When the rolling elements reach the end (position) of the defect (refer to Figure 6 to see the '*ending position of the defect*'), they again come into contact with the non-damaged surface of the cup raceway. At this instance, the contact force on the rolling elements increases from zero to a certain value that is related to the static load distribution on the rolling element.

The resumption of the contact between the rolling elements and the cup raceway results in the re-stressing of the rolling elements. Event # 3, which corresponds to the re-stressing of the rolling elements between the cup and cone raceways, is highlighted using solid rectangular markers on all the subplots in Figure 5.

Prior to regaining the full contact with the raceways, the rolling elements are gradually wedged between the cup and cone raceways. During this period they continuously rattle between the raceways until they are fully loaded. The subplots shown in Figure 5 were zoomed in the vicinity of the re-stressing of the rolling elements, and are shown in Figure 7.

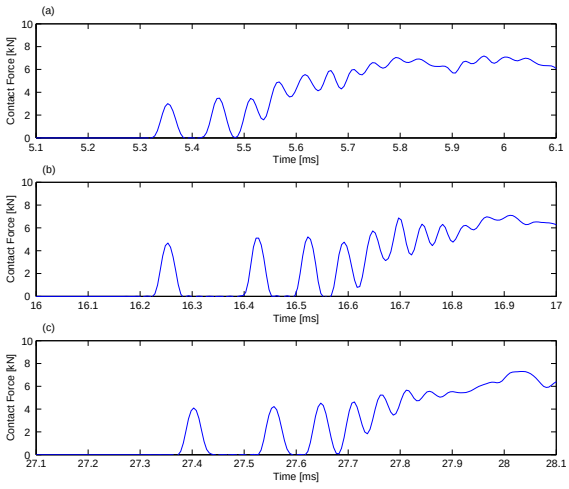

Figure 7: Numerically (LS-DYNA) modelled contact force results shown in Figure 5 are zoomed in the vicinity of the rolling elements being re-stressed between the raceways; (a) cup raceway-rolling element 1, (b) cup raceway-rolling element 2, and (c) cup raceway-rolling element 3.

In contrast to the de-stressing of the rolling elements upon their entrance into the defect where no impacts occur, the contact force plots in Figure 7 show that the exit of the rolling elements from the defect causes a few impacts that can result in the ringing of the bearing.

It is interesting to note that the results of the numerically modelled contact forces show that the amplitude of the impacts produced during the re-stressing phase, approximately 5 kN, is higher than those produced when the rolling elements impact the top surface of the defect, which is less than 2 kN. This is an important outcome of the modelling as it indicates that higher forces and stresses are generated on the exit from the defect compared to when the rolling elements impact the defect surface, and hence could lead to the gradual expansion or lengthening of the defect.

MECHANISM OF DEFECT RELATED IMPACT GENERATION

In order to explain the impact generation mechanism, it is useful to compare the contact forces on the rolling elements with both raceways.

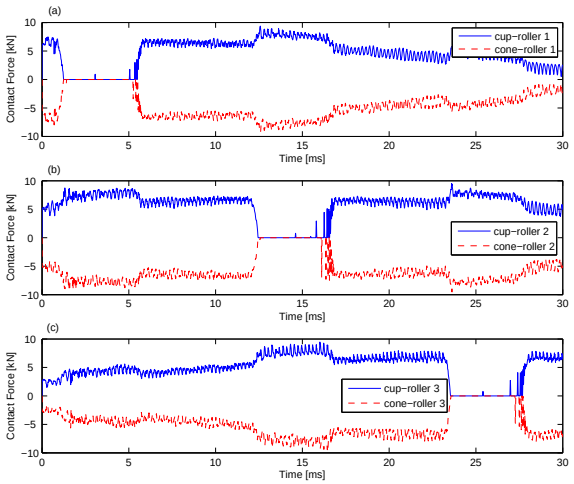

Figure 8: Numerically (LS-DYNA) modelled results for the contact forces between two contact interfaces: 1) cup raceway and the three rolling elements that traversed through the defect; and 2) cone raceway and the rolling elements; (a) raceways-rolling element 1, (b) raceways-rolling element 2, and (c) raceways-rolling element 3.

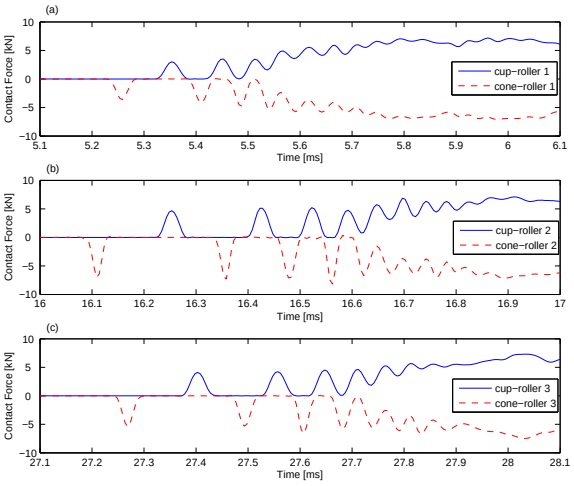

Figure 9: Numerically (LS-DYNA) modelled contact force results shown in Figure 8 are zoomed in the vicinity of the rolling elements being re-stressed between the raceways; (a) raceways-rolling element 1, (b) raceways-rolling element 2, and (c) raceways-rolling element 3.

Figure 8 shows both sets of numerically (LS-DYNA) modelled contact force plots for the three rolling elements as they traverse through the defect. The rolling elements-cup raceway contact forces act in the +y direction, and the rolling elements-cone raceway contact forces act in the -y direction. Figure 8 shows that both sets of the contact forces closely follow each other, however, in opposite directions. It can be seen from Figure 8 that the rolling elements completely lose their contact (fully de-stress) with both raceways at the same instance of time.

Like the re-stressing of the rolling elements observed in Figure 5, the contact force results between the rolling elements and cone raceway also show similar re-stressing behaviour in the vicinity of the end of the defect. For clarity purposes, the contact forces shown in Figure 8 are zoomed in the vicinity of the re-stressing phase, and the corresponding plots are shown in Figure 9. As the rolling elements are re-stressed between the raceways, they impact the raceways alternatively (like a game of ping-pong). The amplitude of the forces on the raceways is higher at the beginning of the re-stressing phase and it reduces gradually as the rolling elements fully stress between the raceways. The alternating pattern of impacts on cup and cone raceways appears as a decaying sine wave.

In summary, defect-related impulses in damaged rolling element bearings are produced during the re-stressing phase, which occurs in the vicinity of the end of the defect, where the rolling elements alternatively impacts the cup and cone raceways.

As the contact forces between the rolling elements and the raceways are not measured in practice, they can be compared with the acceleration results from simulations to correlate the timings of the re-stressing events with the timings of impulses observed in the acceleration results.

Cause of impulsive signals in acceleration results

Figure 10 comprises four subplots; subplot (a) shows the numerically (LS-DYNA) modelled nodal acceleration results (shown in Figure 3), and subplots (b)-(c) show the numerically modelled rolling elements-cup raceway contact forces (shown in Figure 5). Out of the three events discussed above, the time instances corresponding to the occurrences of event #2 and event #3 were correlated between the acceleration and contact force plots. Event #2 and event #3 correspond to the rolling elements impacting the damaged surface of the cup raceway, and the re-stressing of the rolling elements, respectively. These events are highlighted using red-coloured broken elliptical markers and green-coloured solid rectangular markers, respectively in Figure 10.

The acceleration results were zoomed in the vicinity of the second and third impacts, and are shown in Figure 11 as subplots (b) and (c), respectively; subplot (a) in Figure 11 is the same as shown in subplot (a) in Figure 10. Despite the contamination of the numerical results with numerical noise, it can be seen in Figures 10 and 11 that the dominant impulsive signals, visible in the acceleration plots, correspond to the re-stressing of the rolling elements.

During the discussion of the impact-contact analysis, it was also observed that the amplitude of the contact forces related to impacts of the rolling elements with the top surface of the defect (event #2) is lower than those related to re-stressing of the rolling elements between the raceways (event #3). This is also reflected in the acceleration results. The amplitude of the acceleration during the re-stressing of the rolling elements is approximately twice the amplitude of the acceleration during the period where the rolling elements impact the top surface of the defect.

In summary, although a rolling element can impact the surface of the defect and generate a low amplitude acceleration

signal, a much higher acceleration signal is generated when the rolling elements are re-stressed between the raceways.

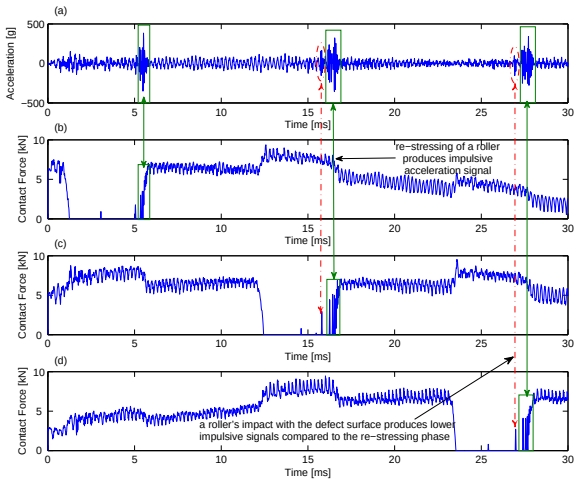

Figure 10: Correlation between the numerically (LS-DYNA) modelled acceleration results shown in Figure 3 and contact forces between the cup raceways and the first three rolling elements that traversed through the defect shown in Figure 5; (a) nodal acceleration, (b) contact force: cup raceway-rolling element 1, (c) contact force: cup raceway-rolling element 2, and (d) contact force: cup raceway-rolling element 3.

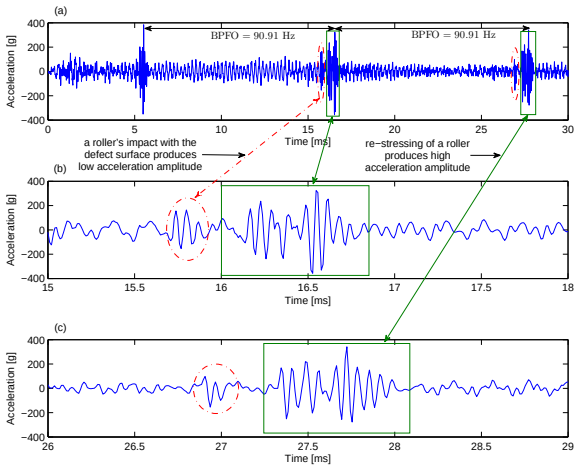

Figure 11: Numerically (LS-DYNA) modelled acceleration results; (a) full time-history showing three impacts which occur during the numerical simulation, (b) partial time-history zoomed in the vicinity of the second impact, and (c) partial time-history zoomed in the vicinity of the third impact.

CONCLUSION

This paper presented results from explicit finite element analysis of a rolling element bearing with a rectangular defect on its cup raceway. The results and interpretation of impact-contact forces between the rolling elements and cup raceway, and rolling elements and cone raceway were presented. The numerically modelled acceleration results were correlated with the rolling elements-cup raceway contact forces. It was found that the re-stressing of the rolling elements between the raceways, in the vicinity of the end of the defect, produces impacts that generate impulses which are observed in the acceleration signals of a defective rolling element bearing. It was found that the contact forces generated during this period are much greater than when the rolling elements strike the surface of the defect, and hence it is likely that this would lead to the gradual elongation and lengthening of a defect.

ACKNOWLEDGMENTS

This work was conducted a part of an ARC Linkage funded project LP110100529.

REFERENCES

Hallquist, J.O. 2006, LS-DYNA Theory Manual

Harris, T.A., Rolling Bearing Analysis, John Wiley & Sons, Fourth edition, 2001

Ho, D. and Randall, R.B., 2000, 'Optimistaion of bearing diagnostics techniques using simulated and actual bearing fault signals', *Mechanical Systems and Signal Processing*, vol. 14, pp. 763-788

McFadden, P.D. and Smith, J.D. 1984, 'Model for the vibration produced by a single point defect in a rolling element bearing', *Journal of Sound and Vibration*, vol. 96, no. 1, pp. 69-82

McFadden, P.D. and Smith, J.D. 1985, 'The vibrations produced by multiple point defects in a rolling element bearing', *Journal of Sound and Vibration*, vol. 98, no. 2, pp. 263-273

Patil, M.S., Mathew, J. Rajendrakumar, P.K. and Desai, S. 2010, 'A theoretical model to predict the effect of localized defect on vibrations associated with ball bearings', *International Journal of Mechanical Sciences*, vol. 52, pp. 1193-1201

Rafsanjani, A., Abbasion, S., Farshidianfar, A., Moeenfard, H. 2009, 'Nonlinear dynamic modeling of surface defects in rolling element bearing systems', *Journal of Sound and Vibration*, vol. 319, pp. 1150-1174

Randall, R.B., Antoni, J. and Chobsaard, S., 2001, 'The relationship between spectral correlation and envelope analysis in the diagnostics of bearing faults and other cyclostationary machine signals', *Mechanical Systems and Signal Processing*, vol. 15, pp. 945-962

Sawalhi, N. and Randall, R.B. 2008a, 'Simulating gear and bearing interactions in the presence of faults Part I: The combined gear bearing dynamic model and the simulation of localised bearing faults', *Mechanical Systems and Signal Processing*, vol. 22, pp. 1924-1951

Sawalhi, N. and Randall, R.B. 2008b, 'Simulating gear and bearing interactions in the presence of faults Part II: Simulations of the vibrations produced by extended bearing faults, *Mechanical Systems and Signal Processing*, vol. 22, pp. 1952-1966

Su, Y.T. and Lin, S.J. 1992, 'On initial fault detection of a tapered roller bearing: frequency domain analysis', *Journal of Sound and Vibration*, vol. 155, no. 1, pp. 75-84

Tadina, M. and Boltežar, M. 2011, 'Improved model of a ball bearing for the simulation of vibration signals due to faults during run-up', *Journal of Sound and Vibration*, vol. 330, pp. 4287 – 4301

Tandon, N. and Choudhary, A. 1997, 'An analytical model for the prediction of the vibration response of rolling element bearings due to a localised defect', *Journal of Sound and Vibration*, vol. 1997, pp. 275-292